Arab J. Nucl. Sci. Appl., Vol. 56, 4, 141-151 (2023)

ISSN 1110-0451

Arab Journal of Nuclear Sciences and Applications

Web site: ajnsa.journals.ekb.eg

(E S N S A)

Influence of Rotating Magnetic Field (RMF) on Dendrite Growth, Mechanical and Elastic Properties of Sn-Cu-Co Lead-Free Solder Alloy

A. M. El-Taher[a,*], H. M. Abd Elmoniem[b] and S. Mosaad[c]

[a] *Physics department, faculty of science, Zagazig University, Zagazig, Egypt*

[b] *High Institutes for Engineering & Technology, Obour, Km21 Cairo/Belbies Rd., Egypt*

[c] *Physics department, faculty of science, Suez Canal University, Ismailia, Egypt*

ARTICLE INFO

Article history:

Received: 28th Dec. 2022

Accepted: 13th Feb. 2023

Available online: 20th May 2023

Keywords:

Sn-Cu-Co alloys;

Microstructure;

Intermetallic Compounds (IMCs);

Mechanical properties;

Rotating Magnetic Field (RMF).

ABSTRACT

Dendritic microstructures are a common issue in casting applications, leading to subpar mechanical properties. A new and innovative approach for combating this problem is through the application of mechanical stirring using an RMF. The solidification microstructures, mechanical and elastic characteristics of Sn-0.7wt%Cu-xCo (where x = 0.05 and 0.5) alloys were analyzed with and without the application of an RMF. The results revealed that, in the absence of an RMF, both solder alloys displayed extensive and undesirable columnar formations of the dendritic β-Sn phase. However, the application of an RMF led to a significant modification of the solidification microstructure, transforming the dendritic β-Sn phase from columnar to equiaxed, resulting in fragmentation of the dendrites. As well, the average size of $(Cu,Co)_6Sn_5$ IMCs was reduced, resulting in successful suppression of the growth rate of IMCs with the use of RMF. Tensile testing showed that the Sn-0.7wt%Cu-0.05Co alloy with RMF exhibited the highest strength across a range of temperatures and strain rates. Additionally, the ultimate tensile strength, yield strength, yield modulus, and elongation percentage of the Sn-Cu-0.05Co alloy with RMF were approximately 29.2%, 31.8%, 29.2% and 7.1% at 25°C higher compared to that of the RMF-free Sn-Cu-0.05Co alloy. By evaluating the Poisson's ratio, Young's modulus, shear modulus, and bulk modulus, it was determined with a high level of confidence that the application of RMF during solidification made the Sn-7Cu-0.5Co alloy more ductile, while the Sn-7Cu-0.05Co alloy demonstrated increased strength compared to their counterparts without RMF.

1. INTRODUCTION

The dendritic microstructure is known to be the most common solid morphological during the solidification of metal alloys, which is a group of primary (λ_1), secondary (λ_2), and often higherorder side arms that establish a complex networks (Fig. 1), in which cavities among dendrites branches filled by IMCs phase [1]. The most theoretical model for the solidification process is an accumulative process of mass and heat transference and is therefore influenced by flows caused by gravity. In recent decades, research under microgravity conditions has shed light on the significance of the fluid flow, which can typically have major impacts on the solidification structures, such as dendrite growth or grain refinement, transformation from equiaxed to globular microstructures, or macrosegregation [2-3]. In metallic cast alloys, the dendrite structure leads to nonuniform properties in the alloy that severely deteriorate its performance and suitability in many applications. Various techniques have been used to control the growth conditions for nondendritic microstructures, such as doping with alloying elements. To increase the mechanical characteristics of metallic alloys, ultrasonic pulsation and electromagnetic/mechanical stirring have been used in the casting process. Magnetic field is positively identified to improve both temperature oscillations and fluid flow, presenting a capable prospect to achieve an improved nondendritic microstructure or macrosegregations, which has previously been studied by several bestselling authors [4].

Corresponding author: ahmedeltaher80@gmail.com

DOI: 10.21608/ajnsa.2023.183687.1704

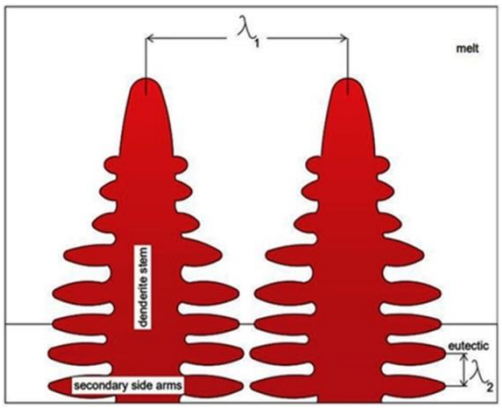

Fig. (1): Definition of primary (λ_1) and secondary (λ_2) dendrite arm spacing [1].

Recently, the rotating magnetic field (RMF) technique has gained much attention in the area of electromagnetic processing of metallic materials. A key advantage of this technique is the ease of treatment and its contactless control on melt flow without contamination [5-6]. Experimental research has demonstrated that RMF exerts a significant influence on the solidification of materials. Zeng et al. [7] adequately investigated the direct influence of RMF on the Sn-Pb alloys during solidification and typically discovered that applying a magnetic field considerably increased flow liquid intensity, and grain refinement and thus enhanced the mechanical properties. Because of the environmental and health concerns associated with a standard Sn-Pb solder alloy, which is very hazardous and cannot be used in electronic applications, numerous lead-free alloy has been established, including Sn-Cu, Sn-Ag, Sn-Bi, and Sn-Zn. Due to their availability, good wettability, high electrical conductivity, and cost-effectiveness, eutectic Sn-Cu solders alloy are carefully considered to correctly be a feasible alternative among all accessible alternatives [8-10]. However, due to the possible formation of a brittle IMCs and the massive main Cu_6Sn_5 crystals in its solder matrix, the wettability and mechanical qualities are widely regarded as poor. Many studies have focused on the gradual incorporation of the notable addition of elements like Bi [11], Co [12], Ni [13], and Al [14] in Sn-Cu alloy. It was discovered that the notable additions of modest amount of Co to the Sn-Cu considerably changed the intermetallic morphologies and its solidification behavior [15]. Tseng et al investigated the effect of minor Co additions in Sn-Cu solders on their interactions with Ni and Cu substrates. They discovered that the addition of 0.01-1 wt.% Co does not affect the reaction pathways of the Sn-Cu/Ni and Sn-Cu/Cu systems but does influence the reaction kinetics [24]. Zeng et al. [25] demonstrated that the microstructure of Sn-0.7Cu was refined by the concurrent addition of Ni and Zn, resulting in the suppression of both Cu6Sn5 and Cu3Sn growth. Ni and Zn were homogenously distributed in Cu6Sn5 intermetallic compounds (IMCs) at the solder/Cu interface, inhibiting the polymorphic phase transformation of Cu_6Sn_5. However, there is a scarcity of systematic data on the direct effects of Co additions in conjunction with RMF on the solidification structures and tensile properties of alloys. However, RMF-modified solidification offers a revolutionary way to enhancing the reliability of solder alloys. In our experimental approach, we have studied the direct influence of possible application RMF during solidification on the fundamental properties of Sn-0.7Cu-xCo (x = 0.05 and 0.5 wt%) solder alloys.

2. EXPERIMENTAL TECHNIQUES

Solder alloys based on Sn-0.7Cu doping with (0.05 wt % Co and 0.5 wt % Co) were synthesized using high purity Sn, Cu, and Co (99.99 % purity), and the composition ratios are indicated in Table (1). For one hour, the melting process was carried out in an electrically heated furnace at 800 °C. The molten metals were immediately exposed to RMF. The magnetic field is generated by attaching a disk-like NdFeB permanent magnet, with a field strength of 0.5 T, to the north and south poles. The permanent magnets measure 60 mm x 30 mm x 20 mm and have their poles situated 30 mm apart. An adjustable speed motor, connected to a power supply, drives the rotating permanent magnets with a rotation speed of 120 RPM, as depicted in Figure 2. Each sample's solution was remelted twice to ensure homogeneity, and the liquid was fluxed in a 1 cm diameter tube and allowed to cool gently at an average cooling rate of 7 $^oC\ s^{-1}$. For mechanical measurements, the samples were extracted to 40 mm in length and 0.8 mm in diameter. To progressively eliminate residual stress caused by sample preparation, the samples have been annealed at 120 ^oC for 45 minutes. The tensile measurements were performed at different temperatures ranging from 25 to 110 ^oC and at strain rates ranging from 10^{-5} to $10^{-3}\ s^{-1}$by using a digitalized tensile machine (Standard ASTM E8/E8M). Solutions of 2% HNO_3, 3% HCl and 95% ethiyle alcohols were produced and utilized to etch the alloys. Field emission scaning electron microscopy (Quanta 250 FEG high resolution) and opticol microcsopy (0M, Carl-Zeiss-Jena-JENAP0L) were used to investigate the morphology and composition of the alloys. For phase identification and structure, all the produced alloys were examined using XRD; (Model

Phillips X'pert) with Cu-Kα radiation (λ=1.54056 Å). The thermal properties of solder alloys were studied by a differential scanning calorimeter [DSC-(STA PT 1000)] at a heating rate of 10 degrees Celsius per minute from 50 to 260 degrees celsius in a He atmosphere. The elastic properties of the soldering alloy were evaluated using ultrasonic nondestructive techniques (PEO), as demonstrated in Figure 3. At ambient temperature, shear wave velocity (VS) and longitudinal ultrasonic wave velocity (VL) were measured using Krautkramer transducer K4KY and KarlDeutsch transducer S12 HB4 with a frequency of 4 MHz. The comprehensive methodology has been documented in previous research [15].

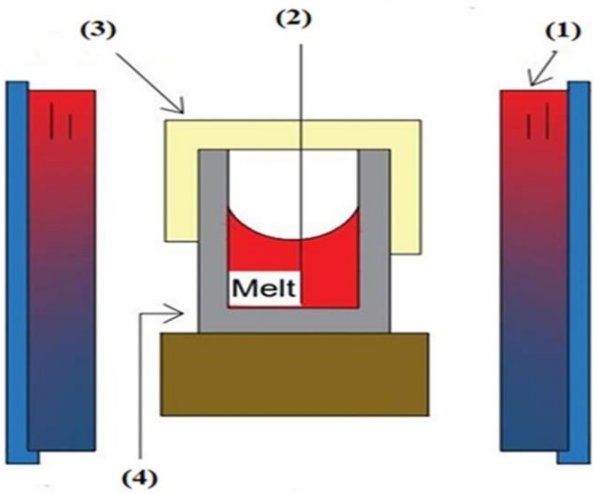

Fig. (2): Schematic diagram of the RMF experimental apparatus: (1) RMF, (2) Temperature recording system, (3) Asbestos and (4) Quartz tube.

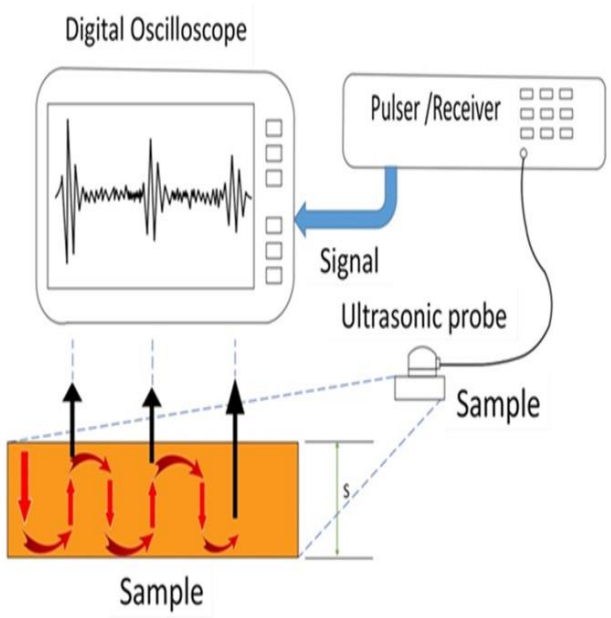

Fig. (3): Schematic representation of the ultrasonic testing (pulse-echo technique).

3. RESULTS AND DISCUSSION

3.1 . XRD analysis

X-ray diffraction (XRD) is a powerful technique for learning about the structure and properties of crystalline materials. This approach not only detects the phases present in a sample, but can also provide more information on the structure of the crystalline phase from the peak profiles, allowing estimation of crystallite size and lattice strain. The XRD patterns of Sn-0.7Cu-xCo (x= 0.05 and 0.5 wt.%) solder alloys solidified with and without RMF are shown in Fig. 4. The interference patterns showed some sharp, narrow and high intensity peaks, which recognized the phase formation of intermetallic compounds produced in the solder alloys. It appears that a large peak intensity of the β-Sn rich phase was formed, while small diffraction peaks of the $(Cu,Co)_6Sn_5$ IMCs phases were detected with variation in the distribution of IMCs in the case of samples without the imposition of RMF. However, a minor distinction in peak intensities was noticed caused by the application of RMF. Additionally, a slight deviation (towards shallower angles) in the positioning of the XRD peaks was observed. This leads to the conclusion that the c-plane of β-Sn crystals is parallel to the direction of magnetic fields. It is understood that when the crystal is subjected to a magnetic field, it seeks to orient itself at an angle that minimizes the overall energy of the system. One plausible explanation for this behavior is that magnetic fields induce β-Sn crystals to rotate towards a position where their c-plane is aligned with the direction of the magnetic field, thereby solidifying in a state of lower energy[16].

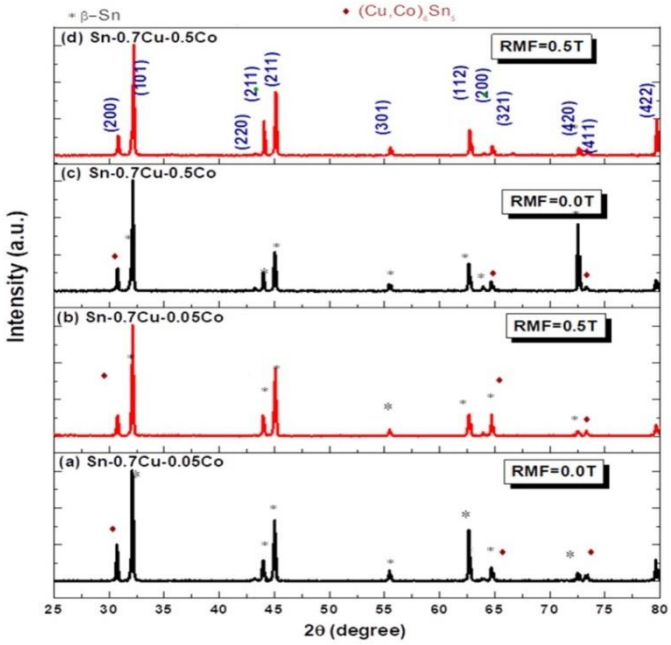

Fig. (4): X-ray diffraction patterns for (a) Sn-0.7Cu-0.05Co, (b) Sn-0.7Cu-0.05Co (with RMF = 0.5 T), (c) Sn-0.7Cu-0.5 Co and (d) Sn-0.7Cu-0.5 Co (with RMF = 0.5 T) solder alloys.

Table (1): Chemical composition of the solders alloys studied (wt. %).

Alloy (Wt.%)	Cu	Co	Pb	As	Sn
Sn-0.7Cu-0.05Co	0.702	0.051	0.001	0.002	Bal.
Sn-0.7Cu-0.05Co RMF	0.701	0.053	0.003	0.002	Bal.
Sn-0.7Cu-0.5Co	0.702	0.520	0.001	0.005	Bal.
Sn-0.7Cu-0.5Co RMF	0.703	0.512	0.003	0.002	Bal.

3.2. Microstructure characterization

Fig. 5 displays the cross-sectional microstructures of Sn-Cu-Co alloys with different Co contents solidified with and without RMF. For the alloys solidified without the imposition of RMF, the microstructure is typically described by a large dendrite morphology of β-Sn grain, and the eutectic phases are more evident and distributed around the β-Sn, consisting of $(Cu,Co)_6Sn_5$ IMCs, as recognized by X-ray technique (Fig. 4). However, the application of RMF during solidification produces a refinement of the eutectic phase, and the dendrite grain aspect is significantly eliminated compared with that before applying RMF, which tends to be more uniformly distributed in the alloys. The application of rotating magnetic fields (RMF) has a noticeable impact on the reduction of β-Sn grain size, which could potentially lead to the fragmentation of dendrite morphologies that are influenced by the force of Lorentz. This serves as an additional nucleation site, contributing to the formation of β-Sn grains and ultimately reducing their size due to the substantial decrease in nucleation energy barriers. Fig. 6 shows the metallographic phase of the solidified alloy with and without applied RMF and its corresponding EDX analysis. The microstructures that crystallized in the investigated alloy involved the main β-Sn phases and interdendritic IMCs $(Cu, Co)_6Sn_5$ phases using an RMF and without an applied RMF during solidification.

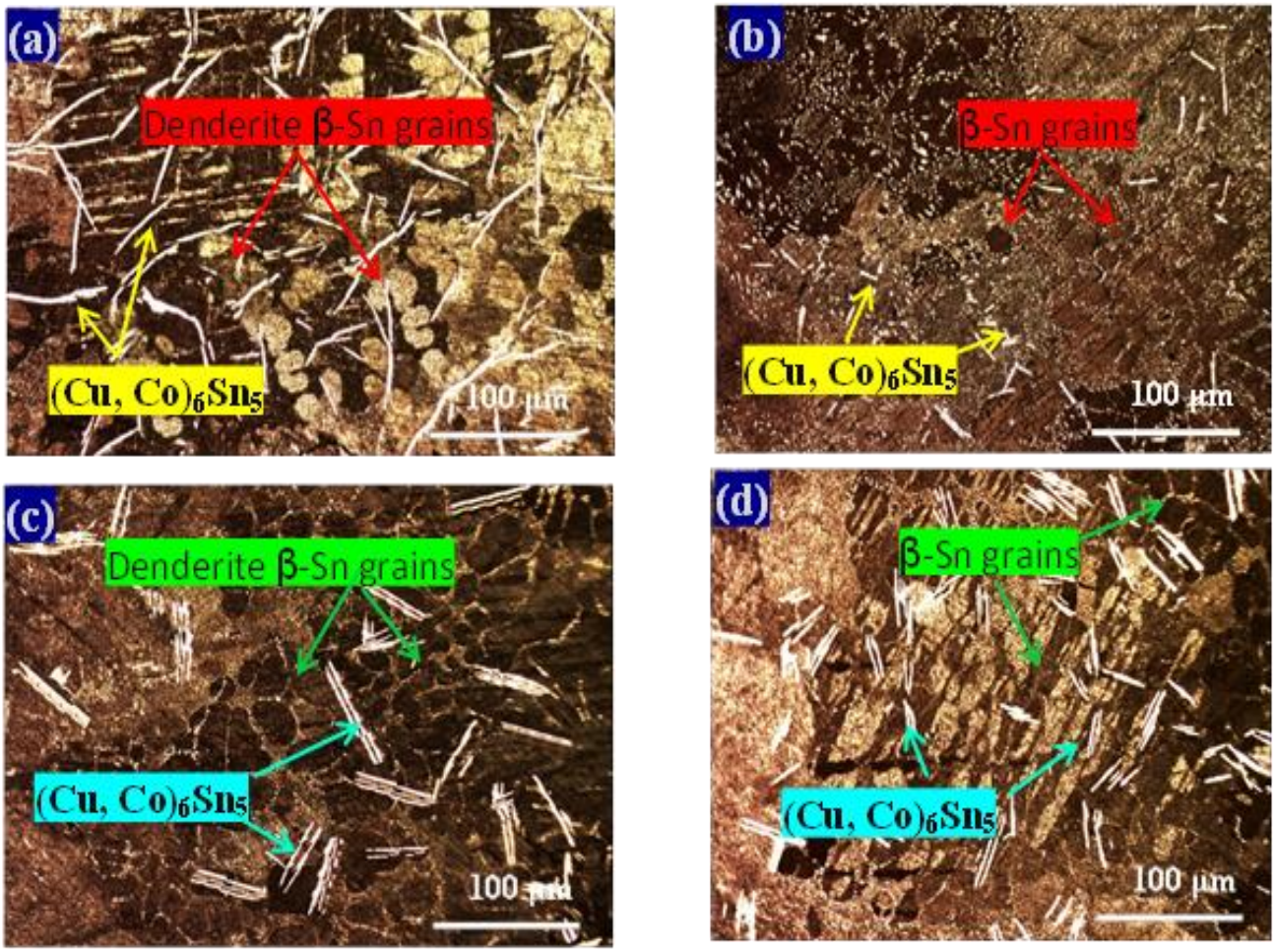

Fig. (5): OM microstructures of solidified (a) Sn-0.7Cu-0.05 Co, (b) Sn-0.7Cu-0.05 Co (with RMF = 0.5 T), (c) Sn-0.7Cu-0.5 Co and (d) Sn-0.7Cu-0.5 Co (with RMF = 0.5 T) solder alloys.

The IMC distribution illustrated in Figure 6a show cases of a predominant presence of β-Sn grains with an inconsistent distribution pattern. Upon enhancing the cobalt ratio ten-fold, as depicted in Figure 6c, the formation of short and coarse fiber-shaped (Cu,Co)6Sn5IMCs becomes apparent. The existence of these phases has the potential to result in a more heterogeneous nucleation process, leading to improved microstructure by reducing the formation of large spheroidal β-Sn grains and altering the solidification process [17]. However, the current RMF altered the phase size, shape, and distribution, as revealed in Fig. 6 (b and d). RMF has a reasonable effect on the optimum dendrite β-Sn grain size in both solders. Dendrites of β-Sn are entirely remelted and refined. Small spheroidal or equiaxed grains form in Sn-0.7Cu-0.05Co and Sn-0.7Cu-0.5Co solder as a result of persistent β-Sn dendritic fragmentation and an increasing amount of nucleation from shattered dendrite formed by the force of Lorentz. In Fig. 6(d), the grain size of β-Sn is progressively reduced, but IMCs are grouped in packages with a nonhomogeneous distribution, which may be attributed to the magnetic characteristics of cobalt. The results reveal that the magnetic field reduces macro-segregation and fragmentation while refining and homogenizing the existing phases. Surprisingly, the originality of the proposed technology will be useful in increasing the thermic and tensile properties of the alloys.

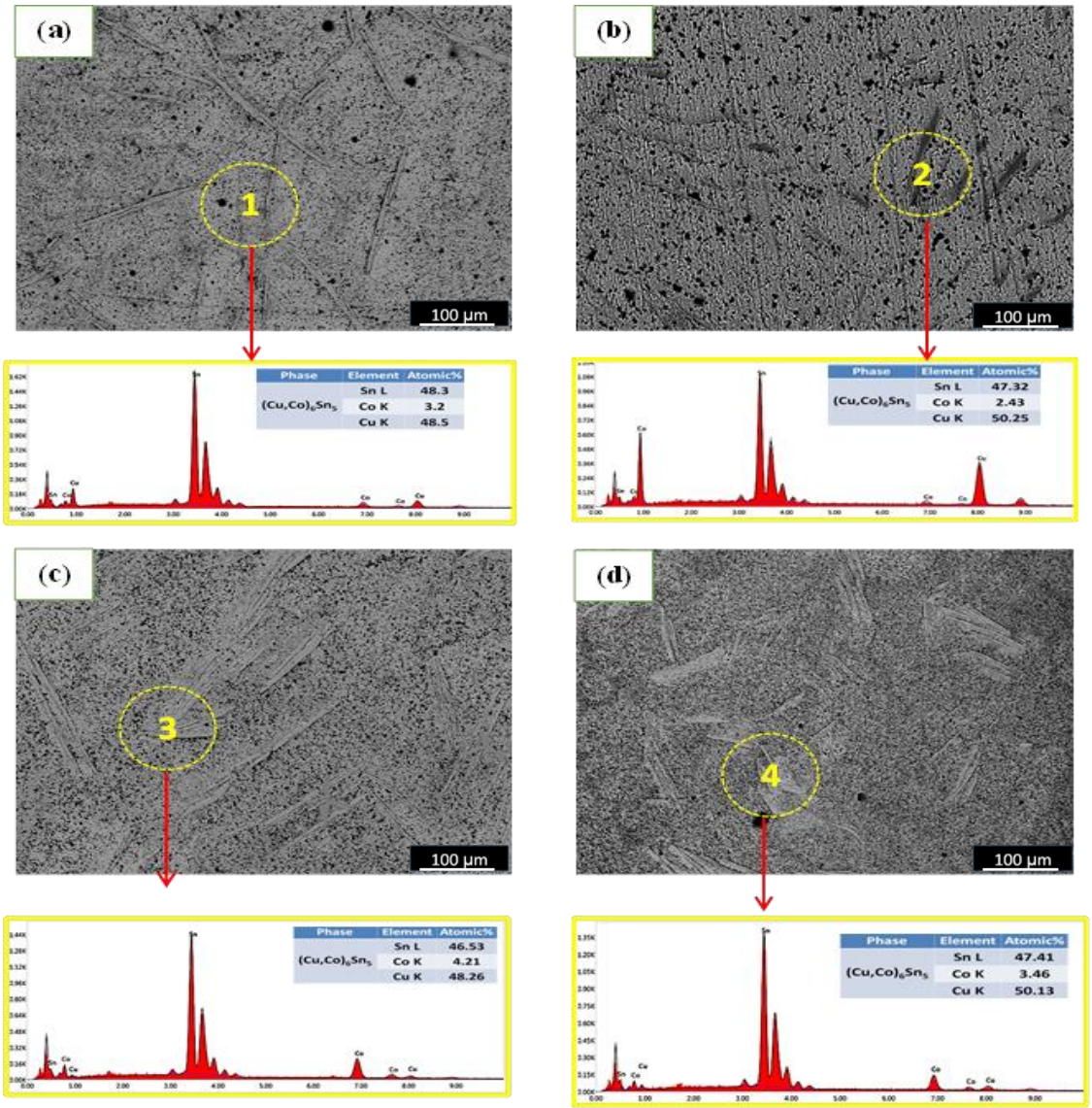

Fig. (6): Typical field emission scanning electron microscopic (FESEM) micrographs of a) Sn-0.7Cu-0.05 Co, (b) Sn-0.7Cu-.05 Co (with RMF = 0.5 T), (c) Sn-0.7Cu-.5 Co and (d) Sn-0.7Cu-.5 Co (with RMF = 0.5 T) solder alloys and it's corresponding EDX analysis.

3.3. Thermal analysis

Fig. 7 represents the heat flow curves for the heating and cooling of the solder alloys Sn-0.7Cu-0.05Co and Sn-0.7Cu-0.5Co with and without RMF. It is clear that the Sn-0.7Cu-0.05Co and Sn-0.7Cu-0.5Co solder alloys both exhibit a single endothermic and exothermic peak. The onset temperatures of the Sn-0.7Cu-0.05Co and Sn-0.7Cu-0.5Co alloys shifted from 222.6 ºC to 220 ºC and from 228 ºC to 220.4 ºC, respectively, because of the MF application during the solidification process, indicating a considerable effect on the kinetics of solidification. The pasty range values for the Sn-0.7Cu-0.05Co and Sn-0.7Cu-0.5Co alloys at RMF = 0 T are 9.2 ºC and 6.6 ºC, respectively, as shown in Table 2. When RMF was applied during solidification, the pasty range values for Sn-0.7Cu-0.05Co and Sn-0.7Cu-0.5Co changed to 7.5 ºC and 9.9 ºC, respectively. The pasty range values for a common eutectic lead-tin solder alloy are less than 11.0 ºC [18]. The researched solder alloys are believed to offer better thermal characteristics because of their smaller pasty range. A reduction in the pasty range enhances soldering quality by eliminating segregation and the occurrence of hot tearing, as well as preventing electronic components from shifting during solidification. It is widely recognized that the melting temperature is a critical factor in determining the maximum operating temperature of a system. Additionaly, Sn-0.7Cu-0.05Co and Sn-0.7Cu-0.5C alloys have T_m temperature values of 226.3 ºC and 231 ºC, respectively. T_m temperatures of Sn-0.7Cu-0.05Co and Sn-0.7Cu-0.5Co were marginally modified by the application of RMF to 221°C and 224 °C, correspondingly.

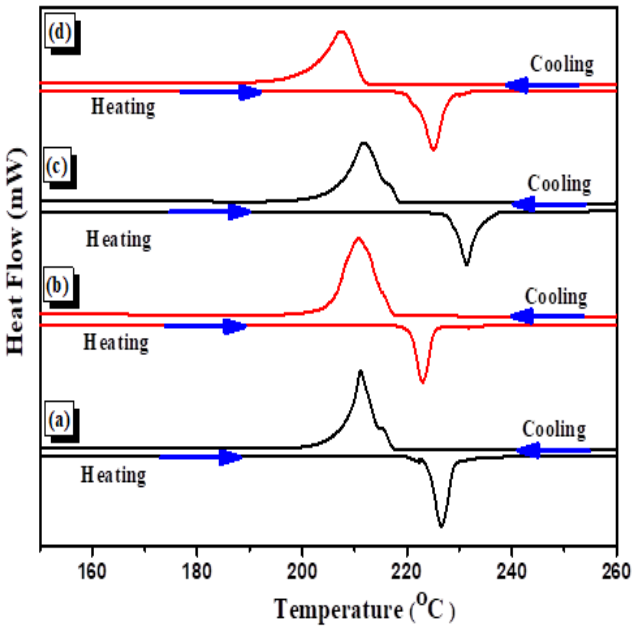

Fig. (7): DSC results for (a) Sn-0.7Cu-0.05 Co ,(b) Sn-0.7Cu-0.05 Co (RMF) , (c) Sn-0.7Cu-0. 5 Co and (d) Sn-0.7Cu-0. 5 Co RMF

Table (2): Pasty range, undercooling, and peak temperature for alloys

Alloy	Pasty range(°C)	Undercooling (°C)	Melting temperature (°C)
Sn-0.7Cu-0.05Co	9.2	6.8	226.3
Sn-0.7Cu-0.05Co RMF	7.5	5	221
Sn-0.7Cu-0.5Co	6.6	12.2	231
Sn-0.7Cu-0.5Co RMF	9.9	9.4	224

The decrease in the melting temperature could result in a wider temperature range for the soldering process and increased soldering ability. Melting point of the solder could be reduced owing to changes in the structural properties of grains feature caused by the application of the RMF, as well as an increase in microstructure instability. Additionally, the support provides information on the soldering procedure since it encourages Sn nucleation, which can result in the improvement of the microstructure. Another aspect that affects the microstructure and crystallization characteristics of solder alloys is undercooling, often known as ΔT. Applying RMF decreased the undercooling for Sn-0.7Cu-0.05Co from 6.8 ºC to 5 ºC along with a drop in the size of the β-Sn grain, as indicated in Table 2, and for Sn-0.7Cu-0.5Co, from 12.2 ºC to 9.4ºC. This shows that the RMF application has a positive impact on undercooling. The mechanical characteristics and microstructure of solder alloys can be affected by little undercooling. The initiation of the β-Sn grains by even a small undercooling may be the cause of the refinements in IMC. The reported T values are within the specified undercooling range of the Sn-Ag-Cu solder alloy, which is 10–30 ºC. This is explained by the fact that β-Sn solidification and nucleation predominantly depend on undercooling.

3.4. Elastic properties

Predicting the general elastic behavior and regional alloy composites deterioration mechanisms, particularly lead-free solders, is a difficult issue because the solder's microstructure influences the deformation behavior. As a result, the modulus of bulk (K), shear (G) and Young (E), as well as coefficient of attenuation (α), Poisson's ratio (υ) and hardness (H) of alloys to externally applied stress may be significant in determining their mechanical characteristics. In Table 3, the accurate data obtained by experimentation of density, longitudinal and shear ultrasonic wave velocities (v_l,v_s) are provided. For the Sn-0.7Cu-0.05Co and Sn-0.7Cu-0.5Co alloys without RMF, v_L was 3449 ± 4 and 3300 ± 4 m/s, while v_s was 1740 ± 11 and 1707 ± 11 m/s,

respectively. It is worth noting that increasing the content of Co addition affects the longitudinal velocity more than the shear velocity due to microstructural change and the creation of coarse fibre $(Cu,Co)_6Sn_5$ IMC in the alloy. When RMF is performed on both alloys throughout solidification, v_l are measured as 3354 ± 4 and 3458 ± 4 m/s, whereas the v_s is 1770 ± 11 and 1576 ± 11 m/s, respectively. A clear shift in the v_l was detected due to the variation in the microstructure of the solder alloy (see Fig. 5). In other words, when RMF was applied, there was little variation in v_s between the Sn-0.7Cu-0.05Co and Sn-0.7Cu-0.5Co alloys. The detected rise or fall in values of the density, on the other hand, should be positively associated with the porosity content, spreading and volume fraction of IMCs phases produced in the tested alloys.

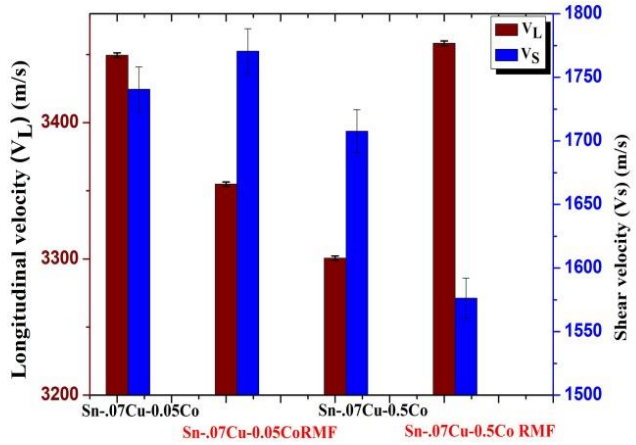

Fig. (8): Ultrasonic wave velocities (longitudinal V_L and shear V_S) values for Sn-0.7Cu-0.05 Co and Sn-0.7Cu-0. 5 Co solder alloys with/without application of RMF.

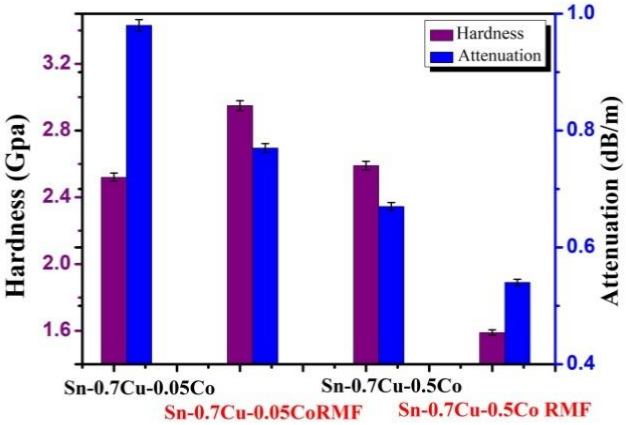

Fig. (9): Hardness (H) and attenuation coefficient (α) values for Sn-0.7Cu-0.05 Co and Sn-0.7Cu-0. 5 Co solder alloys with/without application of RMF.

Hardness is a crucial attribute in solder materials as it reflects the alloy's resistance to plastic deformation. The hardness values of Sn-0.7Cu-0.05Co and Sn-0.7Cu-0.5Co solders are influenced by factors that affect dislocation mobility. The results presented in Figure 9 and Table 4 demonstrate that the application of RMF during solidification results in an increase of hardness value for Sn-0.7Cu-0.05Co from 2.52 ± 0.1 to 3.1 ± 0.1. Conversely, for Sn-0.7Cu-0.5Co, the application of RMF resulted in a decrease of hardness from 2.95 ± 0.1 to 1.59 ± 0.1. The coarse fibre $(Cu,Co)_6Sn_5$ phases in the eutectic structure may result in higher solder matrix hardness of the Sn-0.7Cu-0.5Co alloy prior to RMF than the Sn-0.7Cu-0.5Co sample after RMF as shown in Fig. 5a. As the long fine fiber $(Cu,Co)_6Sn_5$ phases transformed into a short fiber shape with the RMF (Fig. 5b), the solder hardness was diminished. Tan et al. [19] revealed comparable results in their published data, with a small β-Sn phase and improved eutectic installation leading to better (H) of the solder matrix. The estimated findings of (α) in Fig. 9 show that the (α) results of Sn-0.7Cu-0.05Co increased from 0.98 to 1.81dB/m, while it decreased from 0.77 to 0.54dB/m by applying RMF on the solder. The data summarized in Fig. 9 support the suggestion that the attenuations coefficients increases in the Sn-0.7Cu-0.05Co samples after RMF not only because of the microstructural size of the combinations of each solder alloy , but also because of different alterations that occur concurrently as a result of applying RMF. As a result, the declines in intensity of the ultrasonic waves through the entire samples are not recognized from the scattering waves induced by the component of the alloy fluctuation [20]. The coarse fibre (Cu,Co)6Sn5 phases are predicted to have an impact on the intensity decrease of ultrasonic waves after RMF, namely the adjustment of interparticle space and particles size. For technical applications, (Y) and (υ) are crucial factors. They are able to understand how crystalline materials react to outside influences and the connection among structural features and related mechanical effects. The first describes a macroscopically global interpretation of materials stiffness by describing interatomic bonding energies and connections [21-22]. Poisson's ratio, on the other hand, based on compressibility, assesses the material's resistance to expansion and shearing. Its value ranges from (0 to 0.5). The higher υ is, the more ductile is the alloy [7]. Consequently, these studies will provide valuable insights for analysis and alloy design. Figures 10 and 11 depict the Poisson's ratio and elastic moduli of Sn-0.7Cu-0.05Co and Sn-0.7Cu-0.5Co alloys with and without RMF. The application of RMF results in a decrease of Young's modulus for Sn-0.7Cu-0.05Co from 59 ± 0.1 to 56 ± 0.1 GPa, and a decrease from 60 ± 0.1 to 50 ± 0.1 GPa for the Sn-0.7Cu-0.5Co alloy. This suggests that any changes in Young's modulus with or without RMF are inherent to the form, dimension, and distribution of phases and interatomic forces, as well as component connections. Thus, it can be concluded that the elastic modulus in the studied alloys is a result of the microstructural evolution induced by RMF.

Table (3): Ultrasonic Wave Velocities (Longitudinal V_L and Shear V_S) and Density (ρ) of the Solder

Alloy	V_L m/s	V_S m/s	Density kg/m³
Sn-0.7Cu-0.05Co	3449±4	1740±11	7358 ± 5
Sn-0.7Cu-0.05Co RMF	3354±4	1770±11	7343 ± 5
Sn-0.7Cu-0.5Co	3300±4	1707±11	7396 ± 5
Sn-0.7Cu-0.5Co RMF	3458±4	1576±11	7377 ± 5

Table (4): Experimental values of Hardness (H), Young's modulus(Y), Poisson's ratio (y), shear modulus (G), Attenuation coefficient (a) and bulk modulus (K)

sample	(H) Hardness (GPa)	Attenuation (α) (dB/m)	Young modulus (Y) (GPa)	Poission's ratio (υ)	(shear modulus) G (GPa)	(Bulk modulus) K (GPa)	(G/K) ratio
Sn-0.7Cu-0.05Co	2.52 ± 0.1	0.98	59 ± 0.1	0.3292	22 ± 0.1	57.57± 0.3	0.382609
Sn-0.7Cu-0.05Co RMF	2.95 ± 0.1	0.77	60 ± 0.1	0.3069	21.5 ± 0.1	51.78± 0.3	0.415218
Sn-0.7Cu-0.5Co	3.1 ± 0.1	1.81	56 ± 0.1	0.3172	21 ± 0.1	51.05± 0.3	0.411765
Sn-0.7Cu-0.5Co RMF	1.59 ± 0.1	0.54	50 ± 0.1	0.3688	18 ± 0.1	63.51± 0.3	0.283465

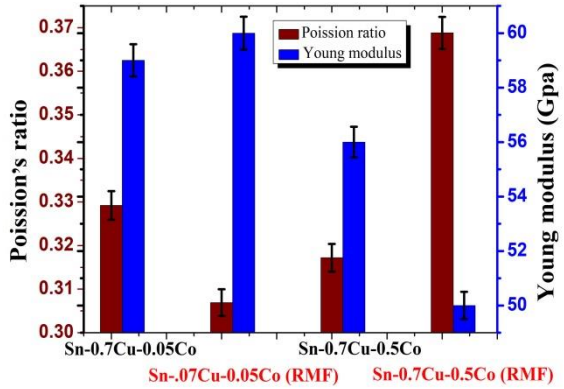

Fig. (10): Poisson's ratio (n) and Young modulus (E) for Sn-0.7Cu-0.05 Co and Sn-0.7Cu-0.5 Co solder alloys with/without application of RMF.

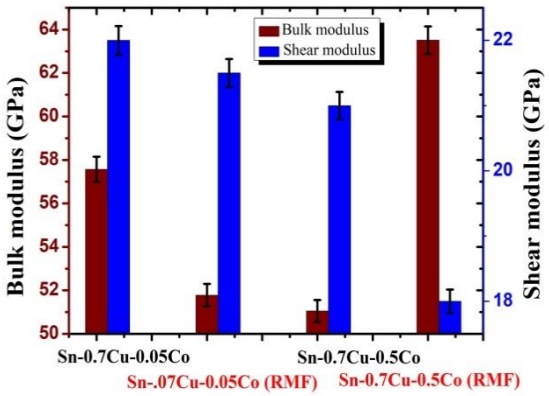

Fig. (11): Bulk modulus (K) and Shear modulus (G) for Sn-0.7Cu-0.05 Co and Sn-0.7Cu-0.5 Co solder alloys with/without application of RMF.

3.5. Mechanical properties

To achieve robust dependability, a solder joint should have high UTS to withstand strong shock loads and thermal stresses. Furthermore, solder joints should be ductile enough to absorb large amounts of mechanical energy before cracks form. Tensile testing was used to evaluate the mechanical properties of Sn-0.7Cu-xCo (x= 0.05 and 0.5 wt.%) solder alloys solidified with and without RMF. Figure 12 shows the stress–strain curves tested at a strain rate of 3.1 x 10^{-3} s^{-1} and at different temperatures (25, 70, and 120 ºc). The mean results of (UTS), (YS), (EL) and (YM) of the alloys have been recorded in Table 5. The figures reveal that all specimens experienced strain hardening rather than strain softening, which can be attributed to the IMC strengthening mechanism in the matrix of the alloys. The recently produced IMC in the matrix of the alloy is operative at typically growing the density of dislocations and removing impediments to dislocation motion, clearly demonstrating the β-Sn dendrites' pinning grain boundaries. According to the scientific data, the Sn-07Cu-0.05Co solder alloy with RMF increases the values of UTS, YS, and YM by 20%, 21%, and 18%, respectively, over the identical sample without RMF. On the other hand, RMF reduces the values of UTS, YS, and YM by 32%, 34%, and 32%, respectively, when

compared to Sn-07Cu-0.5Co without RMF. The results demonstrated a considerable improvement in the tensile characteristics with the use of RMF, resulting in a solder with high strength. It is possible to study the increase in tensile properties brought on by RMF treatment regarding morphological parameters related to grains and secondary phases. The findings of a similar study conducted by A.A. El-Daly et al. [17] demonstrate that incorporating 0.5 wt.% of copper into Sn-20Bi lead-free solder alloys enhances its ultimate tensile strength, yield strength, and Young's modulus, while slightly reducing its ductility. This is attributed to the enhanced accumulation of dislocations at grain boundaries, as well as the promotion of lattice distortion, resulting in a refined microstructure and smaller dendritic β-Sn grain structure, which contributes to the solder alloy's improved tensile strength. The Young modulus (YM) was also investigated, which is definite as linear part the slope of stress-strain curves. Consider the fact that each solder has elastic and plastic reactions at the moment of applied stress when determining (YM). As a result, the (YM) is described as the static modulus, also known as the perceived or functional elastic modulus because the behavior is plainly not fully elastic [23]. When the static modulus results (Table 5) are compared to the dynamic modulus values derived using the ultrasonic wave approach (Table 4), the dynamic Young coefficient values are greater. This typically means that while the static modulus frequently contains modest inelastic distortions or time-dependent deformations like creep, ultrasonic modulus typically excludes inelastic deformation owing to fast wave propagations. As a result, the dynamic modulus calculated typically using the pulse-echo method which is more exact than static modulus accurately calculated using the gentile slope of the stress-strain.

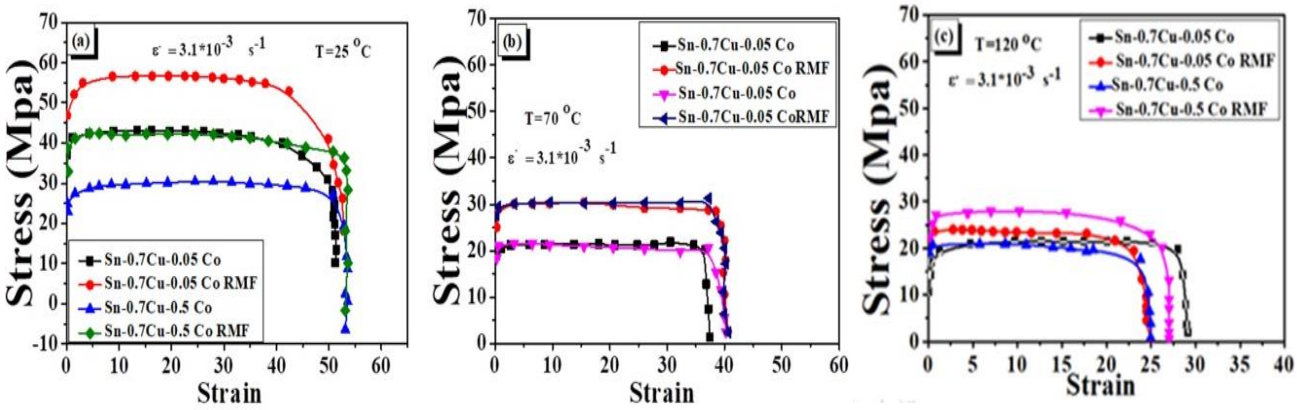

Fig. (12): Tensile Curves for Sn-0.7Cu-0.05 Co and Sn-0.7Cu-0.5 Co solder alloys with/without application of RMF at different strain rates and at different temperature

Table (5): mechanical property data for different solders at $\varepsilon^{\cdot} = 3.1 \times 10^{-3}\ s^{-1}$ and different temperatures.

Alloy	Tempreture (C °)	U.T.S (Mpa)	YS (MPa)	Elongation (%)	Young modulus (YM) (Gpa)
Sn-0.7Cu-0.05Co	25	43.8± 2.5	41.1± 2.5	49± 2.5	21.9± 2.5
	70	21.3± 2.5	21± 2.5	37.5± 2.5	11± 2.5
	110	20.1± 2.5	19± 2.5	28± 2.5	10± 2.5
Sn-0.7Cu-0.05Co RMF	25	56.6± 2.5	54.2± 2.5	52.5± 2.5	28.3± 2.5
	70	31.2± 2.5	29.7± 2.5	40.2± 2.5	15.5± 2.5
	110	23.4± 2.5	23± 2.5	24.8± 2.5	11.7± 2.5
Sn-0.7Cu-0.5Co	25	30.4± 2.5	28± 2.5	53.5± 2.5	15.2± 2.5
	70	22± 2.5	21± 2.5	40.2± 2.5	11± 2.5
	110	21± 2.5	20± 2.5	25.5± 2.5	10.5± 2.5
Sn-0.7Cu-0.5Co RMF	25	42.3± 2.5	41.2± 2.5	56± 2.5	21.2± 2.5
	70	31.8± 2.5	29.5± 2.5	40.7± 2.5	15.7± 2.5
	110	28± 2.5	28± 2.5	27± 2.5	14± 2.5

Figs (12 b and c) show the same behavior at 70 and 110 °c. The temperature dependency of tensile characteristics (YS, UTS, and YM) is remarkable. Rising temperatures clearly degrade the tensile characteristics of Sn-0.7Cu-xCo (x=0.05 and 0.5 wt.%) solder alloys. This is due to the belief that when temperatures rise, dislocations more easily migrate, and the alloy softens, resulting in a drop in tensile strength. On the other hand, low temperatures cause alloy hardening. Clearly, the ductility is slightly raised and subsequently lowered in contradictory ways. This is because of the grain size and strain rate sensitivity parameter.

4. CONCLUSIONS

The following conclusions can be drawn:-

1- The application of RMF fields during solidification influences the growth and distribution of the different phases in the microstructures of Sn-Cu-Co solder alloys.

2- The scientific results designate an imperative refinement of the columnar dendrite behavior of the β-Sn phase and control of the growth of $(Cu,Co)_6Sn_5$ IMCs when RMF is applied to the compositions studied.

3- Applying RMF not only decreased the pasty range and melting temperatures but also reduced undercooling for the Sn-Cu-Co solder alloys.

4- When RMF is applied during solidification, the values of UTS, YS, YM, and El% for Sn-07Cu-0.05Co are increased by 29.2%, 31.8%, 29.2%, and 7.1%, respectively, compared to the same sample without the application of RMF.

5- The elastic modulus is associated with the emergence of new IMC phases. Sn-07Cu-0.05Co with RMF application during solidification was found to be the most favorable due to its higher strength than the other alloys.

ACKNOWLEDGEMENTS

The authors would like to thank prof. Dr. Magdy Elashry for supporting this paper.

REFERENCES

[1] Steinbach, S. and Ratke, L. (2008) Furnace Technology for Experiments on Sounding Rockets: Directional Solidification of Al-cast Alloys in ARTEX", Journal of The Japan Society of Microgravity Application, 25, 467-472.

[2] Glicksman, M.E., Koss, M.B., Bushnell, L.T., Lacombe, J.C. and Winsa, E.A. (1996) Materials and Fluids under low gravity, Lecture Notes in Physics, Eds. Ratke L, Walter H and Feuerbacher B, Springer Verlag, Heidelberg, 6375.

[3] Silva, B.L., Garcia, A. and Spinelli, J.E. (2017) Complex eutectic growth and Bi precipitation in ternary Sn-Bi-Cu and Sn-Bi-Ag alloys, J. Alloys Compd., 691, 600–605.

[4] Zeng, J., Chen, W. and Zhang, S. (2016) Experimental study of molten metal flow and numerical simulation of magnetic field during permanent magnet stirring and its application in continuous casting, Metall. Res. Technol., 113, 609.

[5] El-Taher, A.M., Abd El Azeem, S.E. and Ibrahiem, A.A (2020) Infuence of permanent magnet stirring on dendrite morphological and elastic properties of a novel Sn–Ag–Cu–Sb–Al solder alloy by ultrasonic pulse echo method, J. Mater. Sci.: Mater. Elec., 31, 9630–9640.

[6] Sansan, S., Xin, L., Yuanhao, D., Long, H., Hanlin, L., Jiang, W. and Zhongming, R. (2019) Three dimensional dendritic morphology and orientation transition induced by high static magnetic field in directionally solidified Al-10wt%Zn alloy, materials science & technology, 35, 1587-1592.

[7] Zeng, J., Chen, W. and Zhang, S. (2016) Experimental study of molten metal flow and numerical simulation of magnetic field during permanent magnet stirring and its application in continuous casting, Metall. Res. Technol. ,113,609.

[8] Otsubo, F., Nishida, S. and Era, H. (2014) Solidification structure of Al-Cu and Sn-Cu-Sb alloys obtained by casting through induction stirring using permanent magnet, Mater. Trans, 55, 806-12.

[9] Zeng, J., Chen, W., Yan, W., Yang, Y. and McLean, A. (2016) Effect of permanent magnet stirring on solidification of Sn-Pb alloy, Mater Des, 108,364-73.

[10] El-Daly, A.A., Desoky, W.M., Saad, A.F., Mansor, N.A., Lotfy, I.H., Abd-Elmoniem, H.M. and Hashem, H. (2015) The effect of undercooling on the microstructure and tensile properties of hypoeutectic

Sn–6.5Zn–xCu Pb-free solders, Mater. Des, 80, 152–162.

[11] Salleh, M.A.A.M., McDonald, S.D. and Nogita, K. (2017) Effects of Ni and TiO2 additions in as reflowed and annealed Sn0. 7Cu solders on Cu substrates, J. Mater. Process Technol, 242, 235–245.

[12] Wang, Y., Wang, G., Song, K. and Zhang, K. (2017) Effect of Ni addition on the wettability and microstructure of Sn2.5Ag0.7Cu0.1RE solder alloy, Mater Des, 119, 219–224.

[13] Maeshima, T., Ikehata, H., Terui, K. and Sakamoto, Y. (2016) Effect of Ni to the Cu substrate on the interfacial reaction with Sn-Cu solder, Mater Des, 103, 106–113.

[14] Kanlayasiri, K. and Ariga, T. (2015) Physical properties of Sn58Bi-xNi lead-free solder and its interfacial reaction with copper substrate, Mater Des., 86, 371–378.

[15] El-Daly, A.A., El-Tantawy, F., Hammad, A.E., Gaafar, M.S., El-Mossalamy, E.H. and Al-Ghamdi, A.A. (2011) Structural and elastic properties of eutectic Sn–Cu lead-free solder alloy containing small amount of Ag and In, J. Alloys Compd., 509, 7238-7246.

[16] Jaramillo, R.A, Babu, S.S. and Ludtka, G.M. (2005) Effect of magnetic field on transformations in a novel bainitic steel, Scrip Mater, 52, 461–466.

[17] El-Daly, A.A, Ibrahiem, A.A. and Hammad, A.E. (2018) Impact of permanent magnet stirring on dendrite growth and elastic properties of Sn–Bi alloys revealed by pulse echo overlap method, Journal of Alloys and Compounds, 767,464-473.

[18] El-Taher, A.M., Ibrahiem, A.A. and Razzk, A.F. Viscoplastic characterization of novel (Fe, Co, Te)/Bi containing Sn–3.0Ag–0.7Cu lead-free solder alloy, J. Mater. Sci.: Mater. Elec., 31, 5521–5532.

[19] Tan, A.T., Tan, A.W. and Yusof, F. (2017) Evolution of microstructure and mechanical properties of Cu/SAC305/Cu solder joints under the influence of low ultrasonic power, J. Alloys Compd., 705, 188-197.

[20] Stella, J., Cerezo, J. and Rodrıguez, E. (2009) Characterization of the sensitization degree in the AISI 304 stainless steel using spectral analysis and conventional ultrasonic techniques, NDT&E Int., 42 , 267-274.

[21] El-Daly, A.A. and Hammad, A.E. (2010) Elastic properties and thermal behavior of Sn-Zn based lead-free solder alloys. J. Alloys Compd., 505, 798–800.

[22] El-Daly, A.A., El-Taher, A.M. and Gouda, S. (2015) Development of new multicomponent Sn–Ag–Cu–Bi lead-free solders for low-cost commercial, Mater. Des., 65, 796-805.

[23] Bakhtiar, A., Mohd, F., Mohd, S., Suhana, M.S., Mohammad, H.M., Nazatul, L.S. and Iswadi, J. (2017) Microstructural Modification of Sn-0.7Cu Solder Alloys by Fe/Bi-Addition for Achieving High Mechanical Performance, Journal of Electronic Materials, 46, 4755–4764.

[24] Tseng, Yan-lun; Chang, Ya-chun; Chen, Chih-chi (2015) Co Effects upon Intermetallics Growth Kinetics in Sn-Cu-Co/Ni and Sn-Cu-Co/Cu Couples, Journal of Electronic Materials, 44(1), 581–589.

[25] Zeng G, McDonald S D, Gu Q F (2016) The influence of Ni and Zn addition on microstructure and phase transformations in Sn-0.7Cu/Cu solder joints, Acta Mater., 83, 357-371.